Title: Hypoxia-inducible factor 1 signaling drives placental aging and can provoke preterm labor

Authors: Erin J. Ciampa[1], Padraich Flahardy[1], Harini Srinivasan[2], Christopher Jacobs[2], Linus Tsai[2], S. Ananth Karumanchi[3], Samir M. Parikh[4]

Affiliations:

[1] Department of Anesthesia, Critical Care, and Pain Medicine, Beth Israel Deaconess Medical Center, Harvard Medical School, Boston MA, USA

[2] Division of Endocrinology, Beth Israel Deaconess Medical Center, Harvard Medical School, Boston MA, USA

[3] Department of Medicine, Cedars-Sinai Medical Center, Los Angeles CA, USA

[4] Division of Nephrology, Departments of Medicine and Pharmacology, University of Texas Southwestern Medical School, Dallas TX, USA

Address correspondence to: Samir Parikh, MD. University of Texas Southwestern Medical Center, Department of Internal Medicine. 5323 Harry Hines Blvd. Dallas, TX 75390-9030. Tel: 214-648-2754. Email: samir.parikh@utsouthwestern.edu.

Abstract:

Most cases of pre-term labor have unknown cause, and the burden of preterm birth is immense. Placental aging has been proposed to promote labor onset, but specific mechanisms remain elusive. We report findings stemming from unbiased transcriptomic analysis of mouse placenta, which revealed that hypoxia-inducible factor 1 (HIF-1) stabilization is a hallmark of advanced gestational timepoints, accompanied by mitochondrial dysregulation and cellular senescence; we detected similar effects in aging human placenta. In parallel in primary mouse trophoblasts and human choriocarcinoma cells, we modeled HIF-1 induction and demonstrated resultant mitochondrial dysfunction and cellular senescence. Transcriptomic analysis revealed that HIF-1 stabilization recapitulated gene signatures observed in aged placenta. Further, conditioned media from trophoblasts following HIF-1 induction promoted contractility in immortalized uterine myocytes, suggesting a mechanism by which the aging placenta may drive the transition from uterine quiescence to contractility at the onset of labor. Finally, pharmacological induction of HIF-1 via intraperitoneal administration of dimethyloxalyl glycine (DMOG) to pregnant mice caused preterm labor. These results provide clear evidence for placental aging in normal pregnancy, and demonstrate how HIF-1 signaling in late gestation may be a causal determinant of the mitochondrial dysfunction and senescence observed within the trophoblast as well as a trigger for uterine contraction.

39 **Introduction:**

40 Preterm birth (birth prior to 37 completed weeks of gestation) is a massive global health
41 burden: it leads all causes of death in neonates and children to the age of 5 worldwide[1], and
42 survivors face a broad array of short- and long-term health challenges[2]. Most preterm births in
43 the United States are due to spontaneous onset of preterm labor, with unknown underlying
44 cause[3]. Preterm labor has proven difficult to treat; there currently exist no highly effective
45 interventions that prevent spontaneous preterm birth (SPTB)[4,5]. The dearth of effective
46 treatments stems from our lack of understanding about the pathways regulating spontaneous
47 onset of labor, both preterm and at term.

48

49 The placenta defines the maternal-fetal interface; it is capable of profoundly influencing both
50 maternal and fetal physiology[6-8], and it is subject to remodeling in response to its local
51 environment[9]. Placental disease is known to contribute to other disorders of pregnancy
52 including preeclampsia[10-12] and intrauterine growth restriction[13,14] and there is increasing
53 interest in its potential role as a driver of preterm labor[15-17].

54

55 Recent studies have found that placentas from pregnancies that resulted in SPTB have unique
56 metabolomic and transcriptomic signatures from term counterparts[18-20]. The reported
57 differences broadly implicate the stress response, inflammation, and various metabolic
58 pathways. It has been challenging to narrow these findings or translate them for mechanistic
59 relevance, given the lack of suitable culture systems that integrate experimental manipulation
60 of placental cells with the uterine myocyte response. Furthermore, interpretation studies

61 profiling human placentas from SPTB is sharply limited by the lack of gestational age-matched
62 controls. Without these, the effects of gestational age cannot be distinguished from factors
63 driving premature labor. The placenta encounters a dynamic local environment across its
64 lifetime and faces evolving needs of the growing fetus, so the context of normal gestational
65 age-related changes is vital for the correct interpretation of molecular characteristics
66 distinguishing a SPTB placenta. Defining the molecular-level changes in the *healthy* placenta as
67 it approaches the end of gestation, and their potential effects on the timing of labor onset
68 would therefore address important knowledge gaps.
69
70 Here we report findings from unbiased transcriptomic analysis of healthy mouse placenta,
71 which highlighted hypoxia-inducible factor 1 (HIF-1) signaling as a hallmark of advanced
72 gestational timepoints, accompanied by mitochondrial dysfunction and cellular senescence. We
73 detected some similar effects in human placentas, then modeled HIF-1 induction with two
74 different stimuli and in two trophoblast cell models, demonstrating that mitochondrial
75 dysfunction and cellular senescence arise secondary to HIF-1 stabilization. Whole transcriptome
76 analysis revealed that upon HIF-1 stabilization, a trophoblast cell line acquires signatures that
77 recapitulate the aged placenta. Finally, we show that conditioned media from these cells is
78 sufficient to potentiate a contractile phenotype in uterine myocytes, implicating a mechanism
79 by which the aging placenta may help drive the transition from uterine quiescence to
80 contractility at the onset of labor. This mechanism is further reinforced by an *in vivo* model in
81 which administration of the prolyl hydroxylase inhibitor dimethyloxalyl glycine (DMOG) to

82 pregnant mice induces HIF-1 signaling in the placenta and causes SPTB.

83

84 **Results**

85 To illuminate gestational age-dependent transcriptional changes in across a healthy pregnancy,
86 we collected whole mouse placentas at 48h intervals spanning embryonic day 13.5 to 17.5
87 (e13.5-e17.5) and quantified mRNA and protein targets that emerged from network analysis of
88 an independently published microarray dataset from healthy mouse pregnancies. Upon
89 searching Gene Expression Omnibus (GEO)[21] datasets for "placenta AND transcriptome", we
90 were surprised that among 326 results, only nine included data from normal placenta across a
91 series of gestational timepoints extending to late pregnancy[22-28] (**Figure 1**). We applied
92 weighted gene correlation network analysis (WGCNA) to a microarray study of mouse
93 placenta[22] spanning e8.5 to postnatal day 0 (p0) to assess the mRNA signature of the aging
94 mouse placenta, using the dataset with the best temporal resolution across gestation. Distinct
95 clusters emerged, each reflecting a group of genes whose expression changes across timepoints
96 in a unified way (**Figure 2A;** accompanying statistics available at Mendeley Data, doi:
97 10.17632/g6vrw9jjn4.1). Genes in the 'blue' cluster showed increasingly positive correlation
98 with advancing gestational timepoints; KEGG functional pathways significantly overrepresented
99 among these genes include HIF1 signaling, AMPK signaling, and cellular senescence. Genes in
100 the 'turquoise' cluster showed increasingly negative correlation to advancing timepoints; KEGG
101 functional pathways significantly overrepresented among these genes include the citric acid
102 cycle, mitochondrial complex I biogenesis, and the mitotic cell cycle.

103

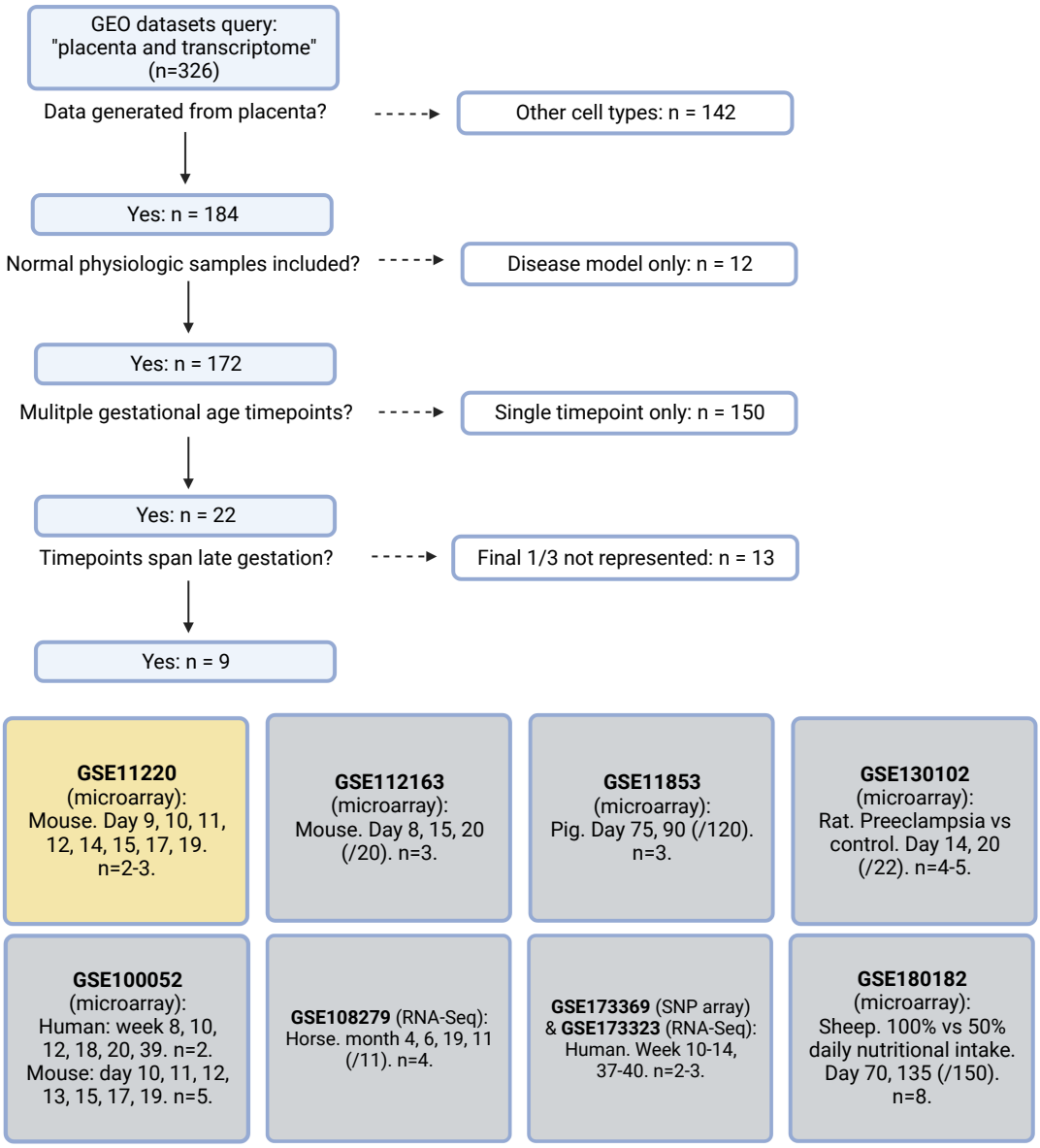

Figure 1. Systematic search flow for placental transcriptomics datasets. 326 GEO datasets were identified by the search terms "placenta" and "transcriptome"; nine met criteria for containing placental transcriptomic data representing normal physiology at a range of gestational timepoints spanning through the final 1/3 of pregnancy. Dataset selected for further analysis in yellow.

104 To validate the dynamic pathway activity suggested by the WGCNA, we quantified mRNA
105 expression of the senescence marker *Glb1*[29] in our mouse placentas, which mirrored the
106 WGCNA finding that cellular senescence in the placenta peaks in the final days of gestation
107 (**Figure 2B**). HIF-1 protein abundance was found to peak at e17.5 (**Figure 2C**) and HIF-1 targets
108 *Hk2* and *Glut1* likewise confirmed increasing HIF-1 activation with advancing gestational age
109 through e17.5 (**Figure 2D**). Of note, a modest but significant fetal sex-dependent difference in
110 HIF-1 target expression (but not *Glb1*) was also observed across timepoints (**Figure 2 -**
111 **Supplement 1**). To assess changes in mitochondrial abundance across gestation, we measured
112 COX IV protein expression and found it declined progressively across mouse gestation (**Figure**
113 **2E**) as predicted by the WGCNA.
114
115 Having observed a pattern of declining mitochondrial abundance in the placenta with advancing
116 gestational age, we next investigated the mitochondrial DNA (mtDNA) lesion rate. The
117 mitochondrial genome is particularly vulnerable to reactive oxygen species (ROS) insults, and
118 mtDNA damage participates in a vicious cycle with mitochondrial dysfunction and further ROS
119 production; these effects are observed in a number of age-related diseases in various tissues[30]
120 and may drive age-associated loss of function[31]. We employed a semi-long run real-time qPCR
121 approach[32] to quantify relative mtDNA lesion rates in mouse placentas, normalized to e13.5.
122 There was a measurable increase in the mtDNA lesion rate in the D-loop and COII/ATPase 6
123 regions of the mitochondrial genome at e17.5 (**Figure 2F**). Together, these results reflect a
124 series of coordinated changes as gestation progresses —namely HIF-1 signaling induction,
125 decreasing mitochondrial abundance, accumulating ROS stress, and escalating cellular

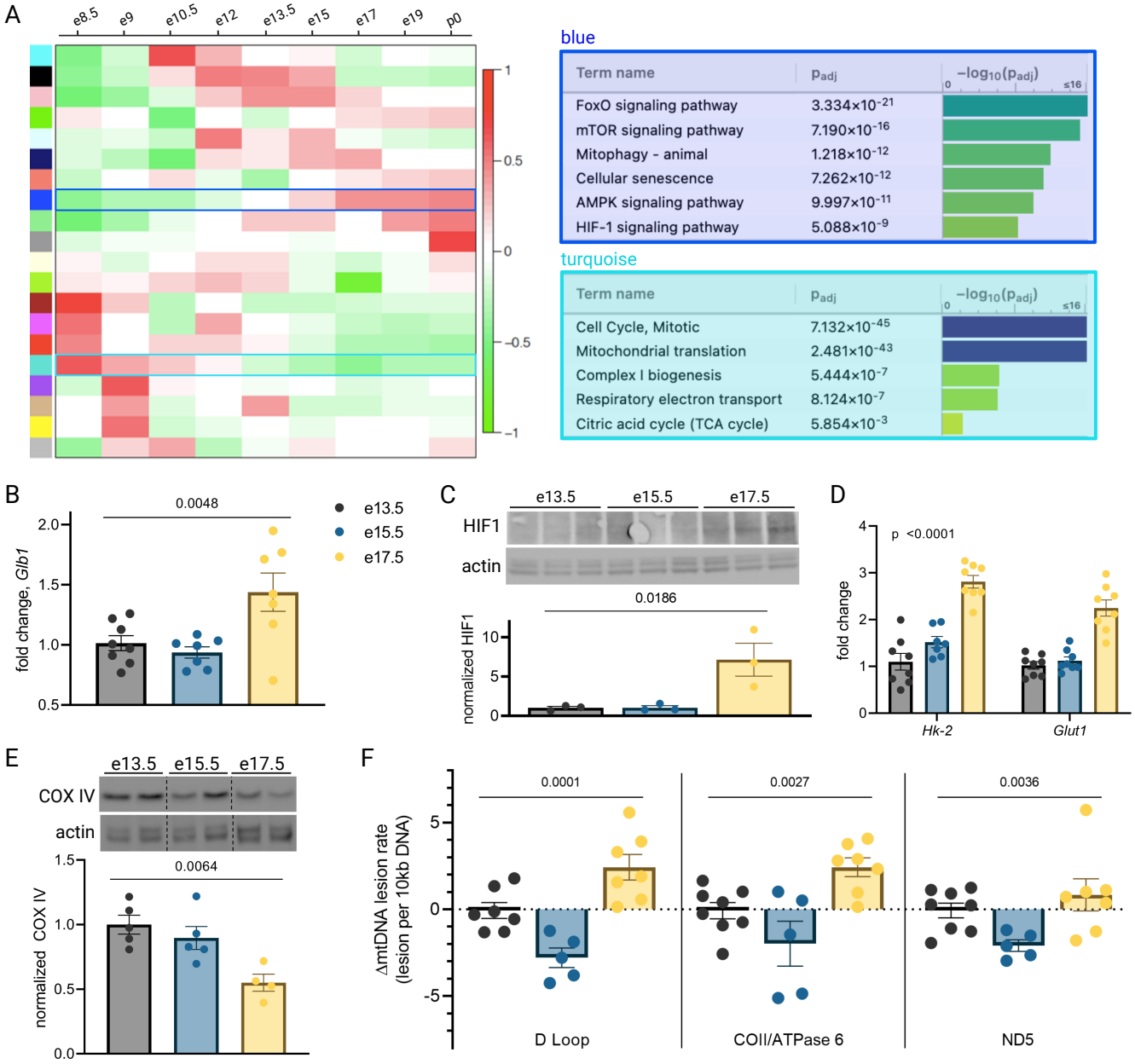

Figure 2. Mouse placental aging is characterized by cellular senescence, HIF-1 signaling, and mitochondrial dysregulation. WGCNA yielded 20 gene clusters. Functional pathways overrepresented in clusters found to increase (blue) and decrease (turquoise) across gestation highlight enhanced cellular senescence, increased HIF-1 signaling, and decreased mitochondrial synthesis and respiration late in pregnancy (A). Expression of senescence marker *Glb1* peaks at e17.5 (B; one-way ANOVA p=0.0048). HIF-1 protein abundance is higher at e17.5 versus e13.5 and e15.5 (C; one-way ANOVA p=0.019), as is expression of HIF-1 targets *Hk2* and *Glut1* (D; two-way ANOVA p<0.0001 for gestational age factor). (See Figure 2 - Supplement 1 for analysis of gene expression changes across timepoints by placental sex.) Mitochondrial abundance, reflected by COX IV protein, decreases with gestational age (E, one-way ANOVA p=0.0064), and mitochondrial DNA lesion rate peaks at e17.5 in the regions of the D-loop (one-way ANOVA p=0.0001), COII/ATPase6 (p=0.0027), and ND5 (p=0.036) (F).

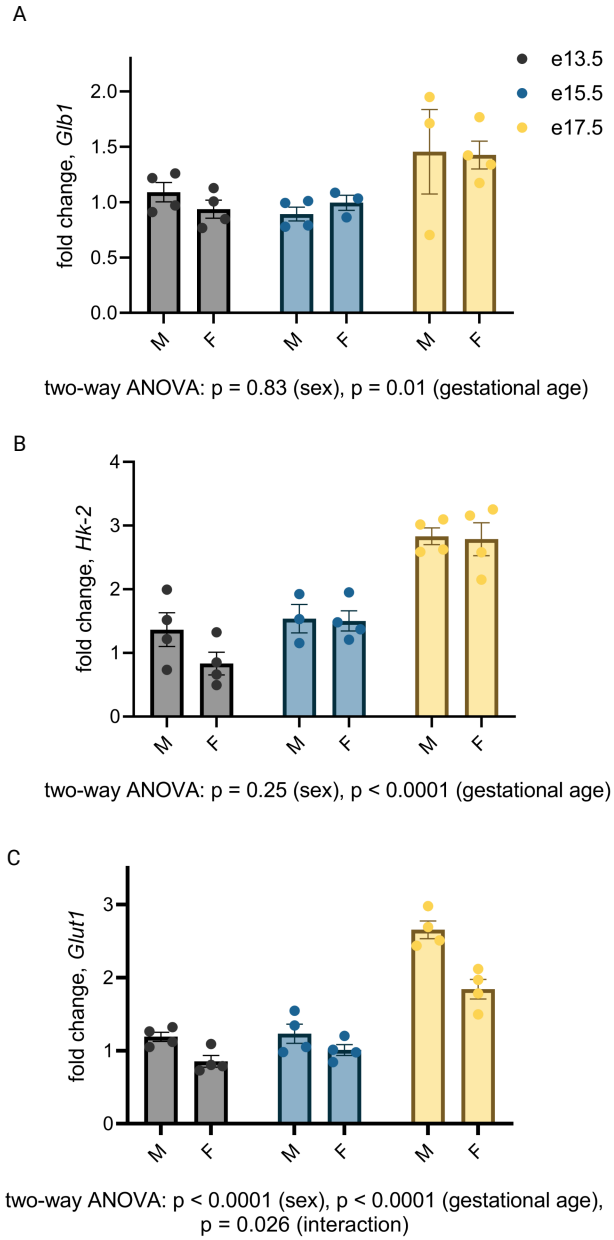

Figure 2 - Supplement 1. Gestational age-dependent variability in expression of Hif-1 target *Glut1*, but not *Hk2*, is affected by placental sex. Subgroup analysis did not reveal sex-dependent expression changes in *Glb1* (A) or *Hk2* (B), but did demonstrate consistently higher *Glut1* expression in male placentas at all gestational ages and an interaction between the effects of sex and gestational age on *Glut1* expression (C; two-way ANOVA p<0.0001 for sex, p<0.0001 for gestational age, and p=0.028 for interaction).

126 senescence — confirming the patterns we discovered through reanalysis of published
127 transcriptomic data.
128
129 We next probed human placentas for the same gestational age-dependent changes. Studying
130 normal human placenta at a range of gestational ages beyond the second trimester is
131 challenging, as placental sampling is usually only possible after delivery, and most deliveries
132 associated with healthy pregnancies occur at term. We therefore sought to capitalize on rare
133 exceptions such as cases of placenta previa, vasa previa, or uterine dehiscence, where
134 iatrogenic preterm delivery is indicated for reasons unrelated to placental health. With an
135 objective to compare term versus preterm placentas, yet minimize confounding factors that
136 accompany labor and disease states that could be expected to affect placental health, we
137 designed a case-control study using the following exclusion criteria: onset of labor prior to
138 delivery (spontaneous or induced); maternal history of hypertension, asthma, diabetes, or
139 autoimmune disease; pregnancy complicated by gestational hypertension, gestational diabetes,
140 preeclampsia, multiples, fetal anomalies, placenta accreta spectrum disorder, or smoking
141 during pregnancy.
142
143 Placentas from 9 cesarean deliveries occurring before 35 weeks gestation and 11 cesarean
144 deliveries occurring after 39 weeks gestation were studied (**Table 1**). Maternal characteristics
145 including race, nulliparity, and obesity were not statistically different across the early versus
146 late groups; there was a small but statistically significant difference in maternal age at the time

	< 35 weeks	> 39 weeks	p value
	n = 9	n = 11	
Gestational age at delivery (weeks)	34.0 ± 0.3	39.5 ± 0.1	< 0.0001
Maternal age (years)	31.9 ± 0.9	36.2 ± 1.0	0.008
Maternal BMI > 40	1 (11)	0 (0)	0.26
Maternal race			
White	7 (78)	9 (82)	0.13
Black	2 (22)	0 (0)	
Asian	0 (0)	2 (18)	
Primiparous	4 (44)	4 (36)	0.71
Female neonate	5 (55)	8 (73)	0.42
Indication for delivery	Placenta previa (3)	Scheduled repeat (7)	
	Vasa previa (4)	Breech presentation (3)	
	Thinned lower uterine segment (2)	Elective (1)	

Table 1. Maternal and fetal characteristics. Data summarized by mean ± SEM or n (%). p-values calculated via t-test (continuous variables) or Chi-square contingency table (categorical variables).

147 of delivery (31.9 ± 0.9 years versus 36.2 ± 1.0 for early gestation versus late, $p = 0.008$). The
148 distribution of fetal sex was not different among groups.
149
150 We found a trend toward increased expression of *GLB1* and HIF-1 targets *HK-2* and *GLUT1* in
151 the > 39-week cohort (**Figure 3A**), consistent with the gestational age-dependent effect seen in
152 mouse placenta. We also examined mitochondrial abundance in the two groups and found that
153 mitochondrial RNA transcripts *ATP6* and *COX2* were significantly decreased (**Figure 3B**) and COX
154 IV protein abundance was lower at the later timepoint (**Figure 3C**), mirroring the mouse
155 findings.
156
157 The co-appearance of cellular senescence, HIF-1 signaling, and mitochondrial dysregulation in
158 the placenta as it approaches the end of gestation led us to hypothesize that in aging placental
159 cells, HIF-1 induction could be upstream of mitochondrial dysregulation and cellular
160 senescence, as is seen in other systems in emerging aging research[33-35]. To test this hypothesis,
161 we established a pharmacological model of HIF-1 induction in primary mouse trophoblasts
162 using cobalt chloride, a prolyl hydroxylase inhibitor that stabilizes HIF-1α[36,37] and has been
163 widely used to model hypoxia. After six hours of $CoCl_2$ exposure, we confirmed HIF-1 protein
164 accumulation in cultured trophoblasts (**Figure 4A**). After 48 hours of $CoCl_2$ exposure, mouse
165 trophoblasts exhibit decreased mitochondrial abundance, by *Cox2* expression (**Figure 4B**) and
166 Cox IV protein abundance (**Figure 4C**), and an increase in senescence-associated beta
167 galactosidase (SA-βGal), encoded by *Glb1* (**Figure 4D**) and detected as a blue stain in an X-gal

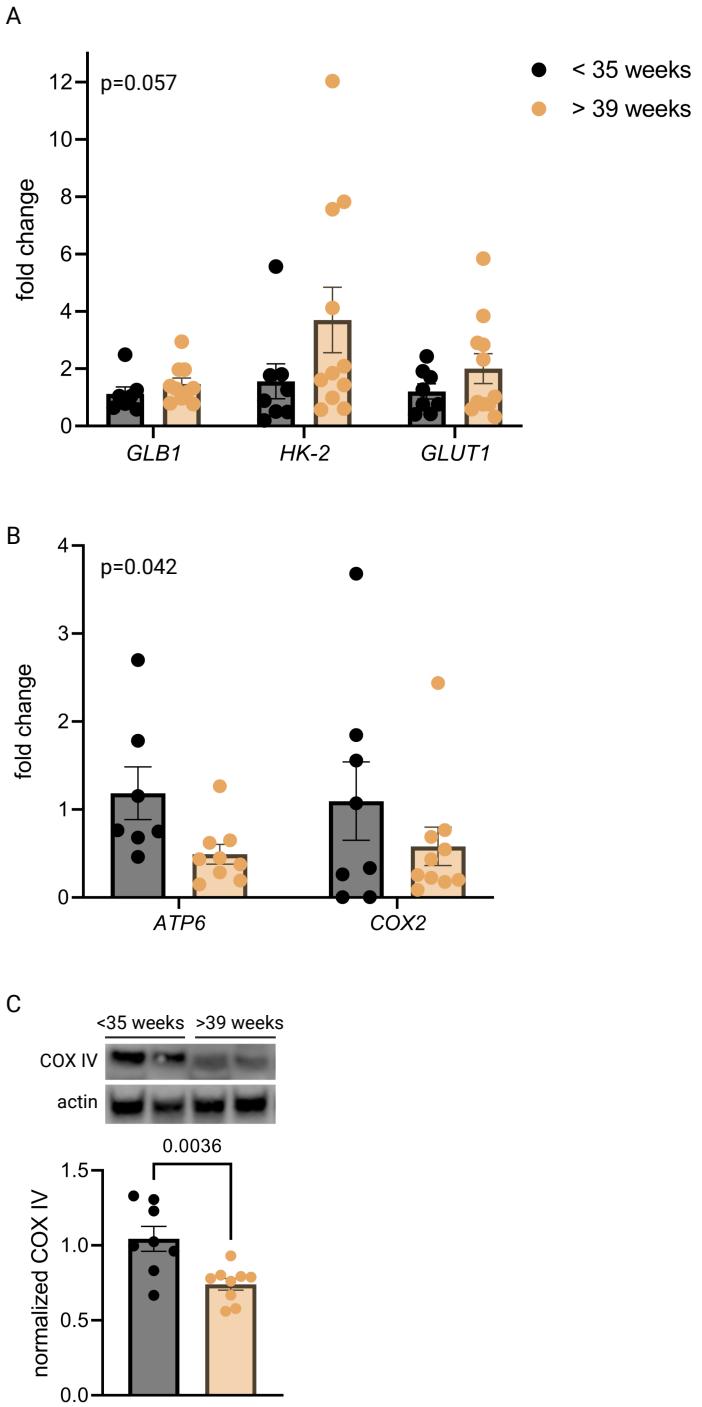

Figure 3. Senescence, HIF-1 signaling, and decreased mitochondrial abundance characterize late-gestation human placenta. Expression of senescence marker *GLB1* and HIF-1 targets *HK-2* and *GLUT1* trends higher in placentas from > 39-week cohort vs < 35-week cohort (A; 2-way ANOVA gestational age factor p=0.057). Mitochondrial abundance, reflected by mitochondrial genes *ATP6* and *COX2* (B; two-way ANOVA gestational age factor p=0.042) and COX IV protein (C; p=0.0036) decreases with advancing gestational age.

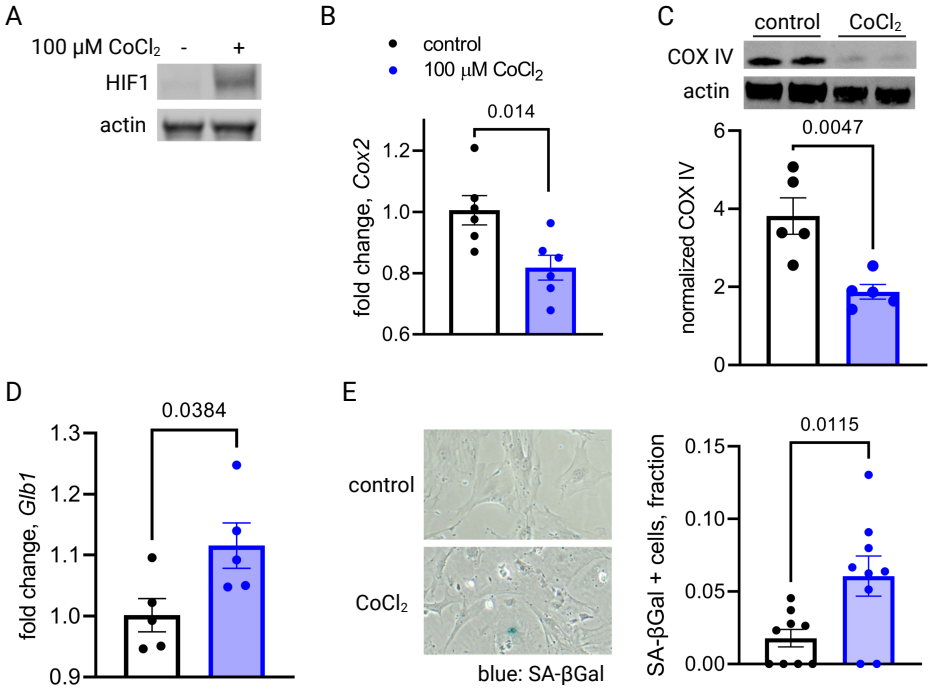

Figure 4. Short-term HIF-1 stabilization in primary mouse trophoblasts leads to decreased mitochondrial abundance and cellular senescence. HIF-1 is detected in cultured trophoblasts exposed to $CoCl_2$ (A). After 48 hours of $CoCl_2$ exposure, trophoblasts exhibit decreased mitochondrial abundance reflected by *Cox2* (B; p=0.014) and COX IV (C; p=0.0047) expression levels. Senescence marker *Glb1* is increased (D; p=0.038) and SA-βGal accumulation is noted by X-gal assay (E; p=0.012).

168 assay for senescence (**Figure 4E**). These findings suggest that HIF-1 stabilization induces
169 subsequent mitochondrial dysfunction and senescence in trophoblasts.
170
171 Primary trophoblasts undergo spontaneous syncytialization in culture, a phenomenon that
172 limits the duration of study and may also confound the interpretation of experimental changes
173 in key metabolic factors[38]. We therefore also modeled HIF-1 activation in JAR cells, a
174 trophoblast cell line that does not undergo syncytialization[39]. Consistent with our results in
175 primary cells, we found that HIF-1 is stabilized in $CoCl_2$-treated JAR cells (**Figure 5A**), and after 6
176 days of exposure, mitochondrial DNA and protein abundance declined (**Figure 5B-C**). We
177 further defined the time course of mitochondrial downregulation: by 72 hours the effect began
178 to appear (**Figure 5 – Supplement 1**). Furthermore, at the 6-day timepoint we found that $CoCl_2$
179 exposure impairs mitochondrial polarization (**Figure 5D**), and leads to accumulation of
180 mitochondrial reactive oxygen species (**Figure 5E**). Additionally, we observed pronounced signs
181 of cellular senescence: morphological hallmarks (cellular swelling) and β-galactosidase
182 overexpression (**Figure 5F**); growth arrest which persists for days after removal of the HIF-1
183 stabilizing compound (**Figure 5G**); and a senescence-associated secretory phenotype (SASP,
184 **Figure 5H**) reflected by increases in expression of VEGF, TNFα and IL-1α and a decrease in the
185 anti-inflammatory cytokine IL-10.
186
187 We conducted additional studies to confirm that cell death was not a primary contributor to
188 the lack of proliferation. Propidium iodide staining with quantitative fluorescence cytometry
189 indicated that $CoCl_2$ treatment only increased cell death by 0-3% (**Figure 5 - Supplement 2**).

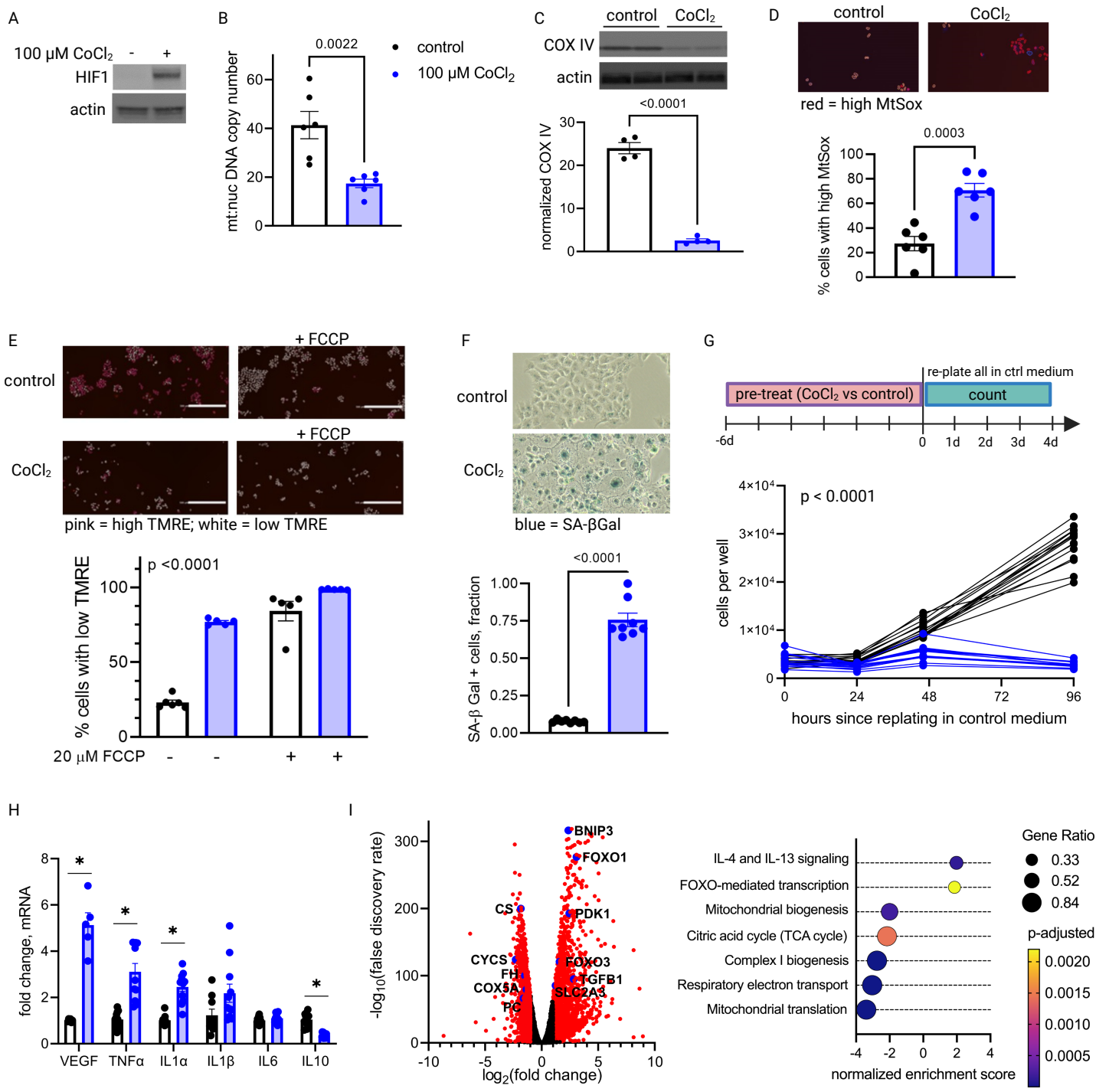

Figure 5. Long-term HIF-1 stabilization in JAR cells leads to mitochondrial dysfunction, cellular senescence, and metabolic reprogramming. JAR cell exposure to $CoCl_2$ stabilizes HIF1 (A). After 6 days, mitochondrial abundance is decreased as reflected by a drop in the mitochondrial:nuclear DNA copy number (B) and a decrease in COX IV protein (C). (See Figure 5 - Supplement 1 for timecourse of COX IV downregulation.) Cells also exhibit augmented signs of mitochondrial dysfunction, including MtSox (D) and TMRE staining (E; two-way ANOVA $CoCl_2$ factor $p<0.0001$). SA-βGal staining reflects a high proportion of senescent cells (F) and growth arrest is confirmed by cell counting following a 6-day pre-treatment with $CoCl_2$ (G; two-way ANOVA $p<0.0001$ for interaction of $CoCl_2$ factor with time). (See Figure 5 - Supplement 2 for assessment of cell death by propidium iodide staining.) SASP candidates VEGF, TNFα, IL-1α, and IL10 are dysregulated after $CoCl_2$ exposure (H; *, adjusted $p<0.01$). RNA Seq revealed upregulation of 2188 and downregulation of 1389 genes (I; genes with $|\log_2(FC)| > 1$ and $-\log(FDR)>2$ indicated in red) after $CoCl_2$ treatment, with geneset enrichment analysis revealing several pathways significantly dysregulated after $CoCl_2$ treatment recapitulating changes seen in transcriptomic analysis of late versus early gestation mouse placenta. Scale marker = 200 μm. See Figure 5 - Supplement 3 for assessment of effects of HIF-1 stabilization in JAR cells using DMOG.

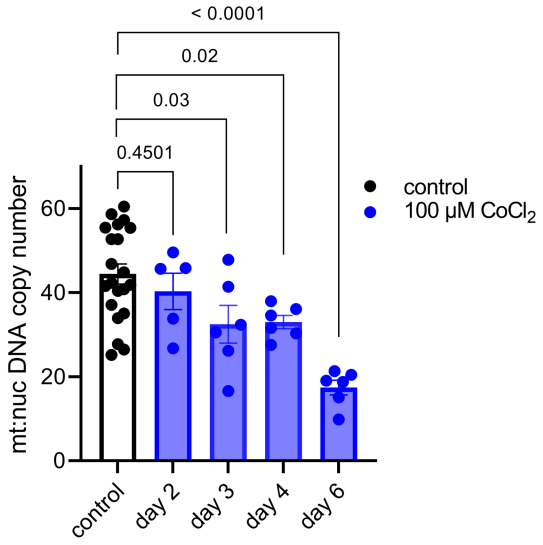

Figure 5 - Supplement 1. The mitochondrial effects of HIF-1 stabilization in JAR cells begin to appear on day 3 following $CoCl_2$ exposure

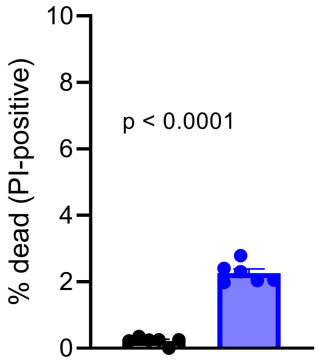

Figure 5 - Supplement 2. Increased number of JAR cells stain with propidium iodide, but the absolute number remains low following 6 days of $CoCl_2$ treatment.

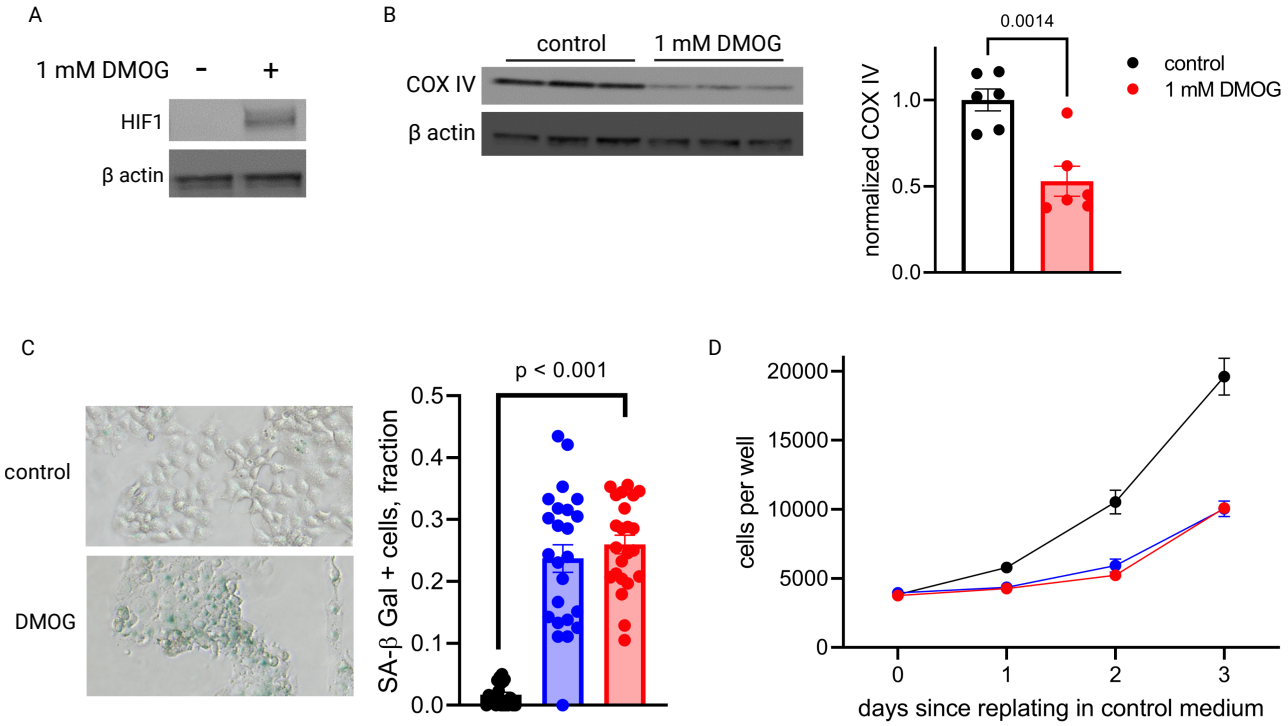

Figure 5 - Supplement 3. DMOG stabilizes HIF-1 in JAR cells (A) and induces similar effects as $CoCl_2$ on COX IV protein (B), SA-βGal expression (C), and cell growth (D) after 4 days.

190 Importantly, cells remained adherent and continued to acidify culture medium beyond 14 days
191 of $CoCl_2$ exposure, providing confidence that HIF-1 stabilization induces a phenotype
192 characterized by predominantly viable cells that are no longer proliferating, namely cellular
193 senescence. Finally, to assess whether the effects we observed were attributable to HIF-1
194 stabilization and not an off-target effect of $CoCl_2$, we also evaluated an alternative prolyl
195 hydroxylase inhibitor, dimethyloxalylglycine (DMOG)[40], and found similar effects on HIF-1,
196 mitochondrial abundance and cellular senescence (**Figure 5 – Supplement 3**).
197
198 To determine if other features of the aged placenta phenotype were recapitulated in this
199 model, we performed whole transcriptome analysis via RNA-Seq. Differential expression ($\log_2$
200 fold change > 1; FDR < 0.05) was found for 2188 upregulated and 1389 downregulated genes
201 (**Figure 5I**). Gene set enrichment analysis revealed that chemical hypoxia led to upregulation of
202 inflammatory signaling, and downregulation of the TCA cycle, mitochondrial biogenesis, and
203 respiratory electron transport. These data therefore recapitulated metabolic patterns that
204 emerged from time course transcriptomic analysis of intact placentas (Figure 2A).
205
206 The onset of labor is accompanied by a transformation of the uterus from quiescence into a
207 distinct physiologic state in which it generates powerful, coordinated contractions. This
208 phenotypic change is characterized by upregulation of a cadre of contraction associated
209 proteins (CAPs), notably: cyclooxygenase-2 (COX-2, encoded by *PTGS2*), prostaglandin F2α
210 receptor (encoded by *FP*), interleukin-6 (IL-6), and connexin 43 (Cx43, encoded by *GJA1*)

211 Phenotypic switching can be modeled in primary and immortalized uterine myocytes upon
212 stimulation with inflammatory mediators such as IL1β, PGF2α, and thrombin[41-43].
213
214 To test whether primary placental metabolic disruptions could crosstalk with uterine myocytes
215 to trigger the contractile phenotype, we collected conditioned media from our JAR cell model
216 of HIF-1-driven senescence and measured the effect on expression of CAPs in uterine myocytes
217 (hTERT-HM cells). We observed a robust and specific effect: co-stimulation of uterine myocytes
218 with IL-1β plus conditioned media from JAR cells treated with $CoCl_2$ (but not from untreated
219 JAR cells) potentiated the induction of *PTGS2*, *GJA1*, *FP*, and *IL-6* expression (**Figure 6A-D**). We
220 next employed a collagen lattice assay previously described for assessing contractility of
221 myometrial cells *in vitro*[41,44], and demonstrated that myocyte contraction is augmented upon
222 exposure to conditioned media from JAR cells treated with $CoCl_2$ but not from untreated JAR
223 cells (**Figure 6E**). These transcriptional and functional results collectively demonstrate that
224 uterine myocytes are responsive to the secretome of JAR cells driven to senescence via HIF-1
225 induction.
226
227 To test whether HIF-1 induction drives labor onset *in vivo*, we administered DMOG
228 intraperitoneally to pregnant mice on gestational day e16.5. Analysis of placentas recovered 12
229 hours following injection indicated that HIF-1 protein is stabilized in placenta following
230 maternal DMOG injection (**Figure 7A**), and transcription of HIF-1 target genes *Hk-2* and *Glut1*
231 was significantly increased (**Figure 7B**). Following injection of DMOG, gestational length was
232 significantly shortened compared to injection of vehicle alone (**Figure 7C-D**).

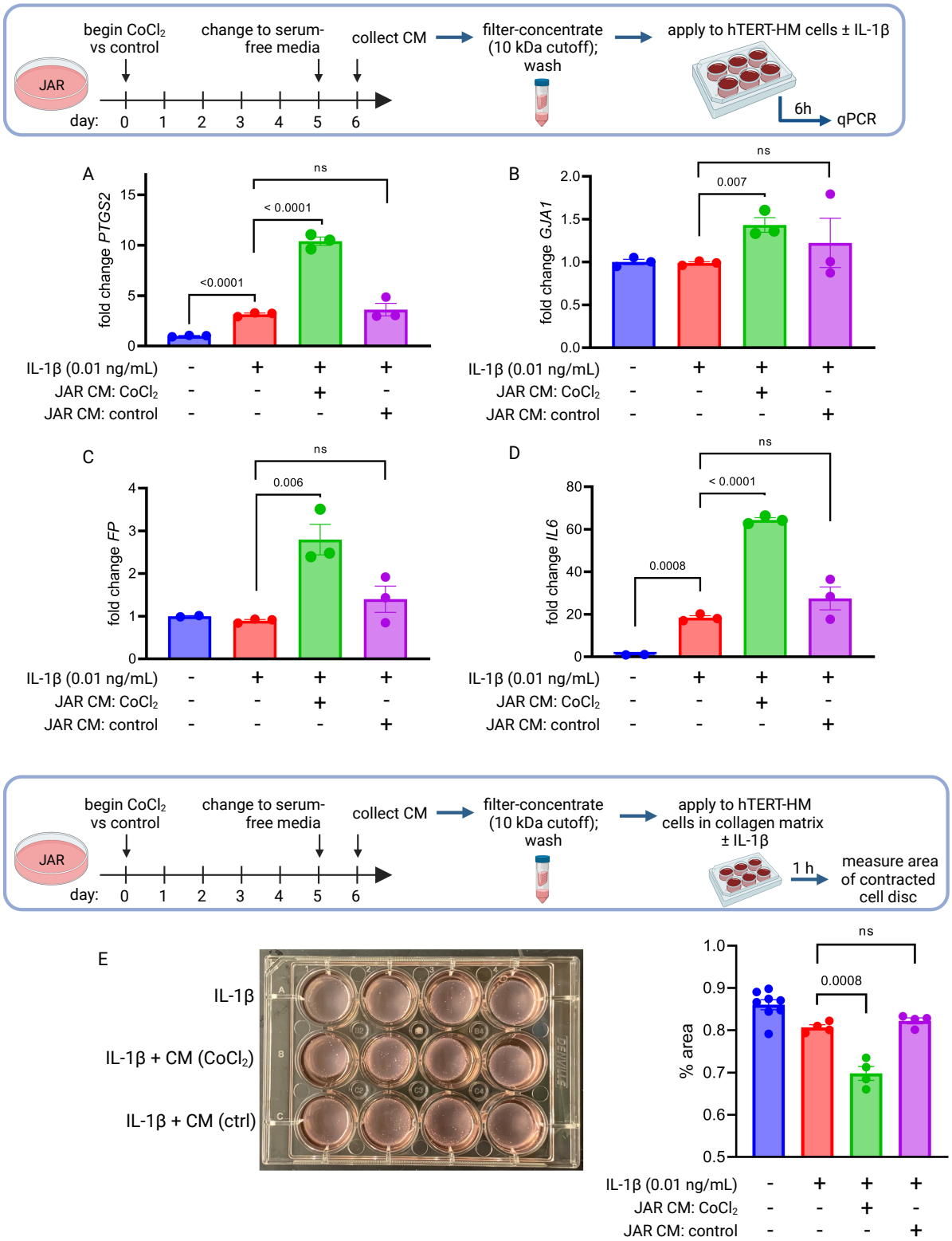

Figure 6. Conditioned media (CM) from JAR cells following HIF-1 stabilization induces expression of contractile-associated proteins and augments contraction in immortalized human uterine myocytes. hTERT-HM expression of *PTGS2* (A), *GJA1* (B), *FP* (C), and *IL6* (D) was induced by CM from JAR cells following $CoCl_2$ treatment (but not in control conditions), similar to (in some cases potentiating) the effect of stimulation of myocytes by exogenous IL-1β. Percent well area occupied by hTERT-HM cells embedded in collagen matrix is significantly smaller after stimulation with IL-1β plus JAR CM from $CoCl_2$ condition, reflecting greater degree of hTERT-HM cellular contraction (E).

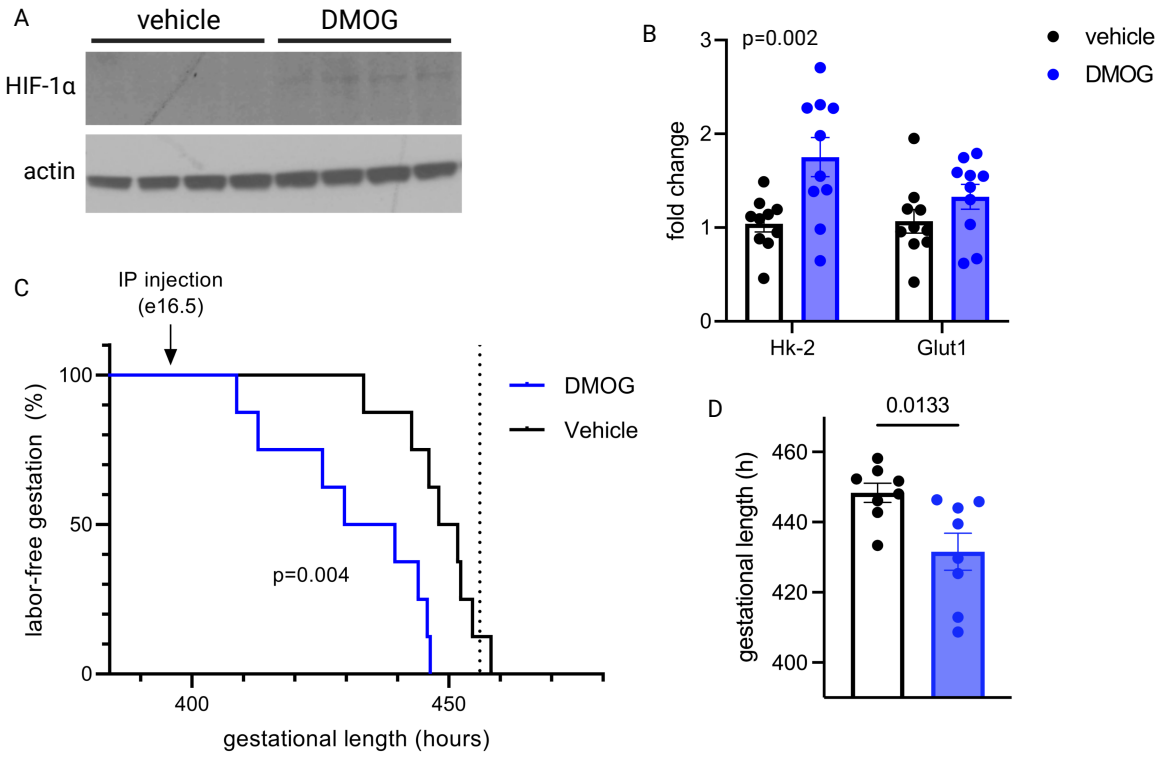

Figure 7. Maternal DMOG injection on e16.5 stabilizes placental HIF-1 and induces preterm labor. HIF-1α protein is detected in placental lysates 12 hours following DMOG injection but not vehicle (A). HIF-1 targets *Hk-2* and *Glut1* are upregulated following DMOG injection (p = 0.002 for DMOG vs vehicle, two-way ANOVA) (B). Gestational length is significantly shortened following DMOG injection versus vehicle (C-D).

233

234 **Discussion**

235 The subject of whether the healthy placenta undergoes aging (with accompanying dysfunction)
236 within its 40-week lifespan has been of great interest and debate for many years. Age-related
237 functional decline is a near-universal phenomenon affecting many tissues, but the underlying
238 biochemical driving factors vary widely depending on the context of cell type and local
239 stressors. Mechanisms well described in other tissues are rooted in genomic instability,
240 mitochondrial dysfunction and oxidative stress, nutrient deprivation and metabolic
241 insufficiency, or loss of proteostasis[45]. While characterization of the placenta as an aging organ
242 appeared in the literature beginning nearly fifty years ago[46,47], a counter-argument has been
243 offered that there is no logical reason for the placenta to undergo accelerated aging relative to
244 the fetus, since both share the same genes and environment[48]. A third viewpoint proposes that
245 aging in the placenta is indicative of a disease state—not normal progression of healthy
246 gestation—one usually reflective of maladaptive responses to oxidative stress[49-53]. Finally,
247 recent reports have noted prominent signs of aging in another fetally derived tissue, the
248 chorioamniotic membranes, in healthy pregnancies[54], and have linked aging of the fetal
249 membranes to the onset of labor[55,56]. The results presented here span mouse and human
250 placentas to provide evidence for placental aging in normal pregnancy. Mechanistic dissection
251 of this phenomenon further demonstrates how hypoxia in late gestation may be both a causal
252 determinant of mitochondrial dysfunction and senescence observed within the trophoblast as
253 well as a trigger to induce uterine contraction.

254

255 To our knowledge, this is the first report to propose that placental aging in healthy pregnancy is
256 characterized by induction of HIF-1 signaling, accompanied by downstream effects including
257 mitochondrial dysfunction and cellular senescence. These findings have implications for the role
258 of the placenta in signaling that promotes the onset of labor, particularly given our
259 demonstration that upon HIF-1 stabilization, trophoblasts can induce inflammatory changes in
260 uterine myocytes and potentiate their contractility, and our *in vivo* demonstration that
261 administration of DMOG stabilizes placental HIF-1 and leads to preterm labor in mice.
262 Important next steps prompted by this work include determining the specific components of
263 the secretome of HIF-1-activated trophoblasts which are responsible for inducing myocyte
264 transformation. Additionally, having established that HIF-1 signaling is upstream of
265 mitochondrial dysfunction and cellular senescence in late-gestation trophoblasts in normal
266 pregnancies, future studies can investigate whether factors that modulate this pathway could
267 increase or decrease vulnerability to preterm labor. In studies targeted to uterine decidua, a
268 link between cellular senescence and labor onset has previously been established, with
269 evidence implicating phospho-Akt and mTORC1 signaling upstream of prostaglandin synthesis
270 as a key mechanism in this model[57,58]. It is possible that senescence signaling from the placenta
271 and decidua converge, and labor is provoked upon these convergent endpoint signals
272 surpassing a threshold, regardless of their origin within the gestational compartment.
273
274 Our results suggest that placental HIF-1 becomes stabilized late in gestation, and this could be
275 secondary to the onset of hypoxia sensing as oxygen demand outstrips supply in the
276 fetoplacental unit. However, placental hypoxia has been difficult to examine *in vivo*. Despite

277 evolving approaches for measurement of placental oxygenation, findings have varied widely
278 and adequate spatiotemporal resolution has so far been challenging[59]. However, it is apparent
279 that due to arteriovenous shunting and high metabolic extraction rates, the placenta
280 experiences hypoxia throughout pregnancy with a reported partial pressure of oxygen 30-50
281 mm Hg in the intervillous space, so perhaps a relevant question is what *prevents* HIF-1
282 stabilization and its downstream effects early in gestation. It is possible that the gestational-
283 age-dependent HIF-1 induction we observed reflects not a change in oxygen availability, but
284 rather a change in other HIF-regulatory factors such as nicotinamide adenine dinucleotide
285 (NAD^+) depletion, as has been demonstrated to occur in muscle and is accompanied by
286 metabolic reprogramming and mitochondrial decline[60]. Importantly, replenishment of NAD^+
287 was shown to restore markers of mitochondrial function in these aged cells, suggesting that
288 mitochondrial effects of HIF-1-driven aging are reversible in some systems. Separately, a recent
289 study which compared the miR-nomes of 1st- versus 3rd-trimester human placenta highlighted
290 differential expression of miRNAs with functional links to silencing of hypoxia response and
291 cellular senescence pathways in the first trimester[61]. Future investigations into the impact of
292 placental HIF-1 regulation will require a more precise understanding of placental oxygenation *in*
293 *vivo* and a sophisticated approach to model these factors in placental explants or other cellular
294 systems.
295
296 The shift in metabolic phenotype away from oxidative respiration in late pregnancy as
297 demonstrated by our transcriptomics analysis is consistent with earlier findings from
298 respirometry studies in mouse placenta[62], where rates of oxidative phosphorylation were noted

299 to decline from e14 to e19, particularly in the labyrinthine zone. It is still unclear if this shift
300 reflects changing substrate availability, or oxygen content, or perhaps the metabolic needs of
301 the developing fetus. A better understanding of the dynamic metabolism of the placenta across
302 gestation will be crucial for developing strategies for optimizing placental health, with major
303 implications for both maternal and fetal outcomes. For example, placental metabolomics
304 studies with a gestational time series could help corroborate the metabolic implications
305 interpreted from our transcriptomic data, while single-cell transcriptomics across advancing
306 gestational age in healthy placentas would offer critical cell-type localization of specific
307 metabolic events noted to occur late in pregnancy. Future studies aimed at targeted
308 manipulation of placental metabolism *in vivo*, whether pharmacologically or genetically, are
309 needed to define the physiologic relevance of these findings.
310
311 Our data have implications for other adverse pregnancy outcomes beyond preterm birth,
312 including intrauterine growth restriction and preeclampsia. An important study previously
313 examined mice with placental expression of a constitutively active HIF-1 mutant and found that
314 when induced from the beginning of gestation, placental HIF-1 signaling drives abnormal
315 placentogenesis and impaired spiral artery remodeling, leading to placental hypoperfusion,
316 fetal growth restriction, and a preeclampsia-like clinical syndrome[63]. In the context of these
317 earlier results, our study highlights the critical gestational age-dependence of HIF-1 effects,
318 having demonstrated that in a normally developed mouse placenta, induction of HIF-1 signaling
319 during the final days of gestation leads to labor onset. Timing may be key to understanding how

320 two distinct pregnancy complications – preterm labor and preeclampsia – appear to emerge
321 separately from overlapping pathophysiologic mechanisms[64-68].
322
323 In summary, we report a molecular characterization of placental aging phenomena occurring in
324 normal pregnancies, stemming from induction of HIF-1 signaling and downstream
325 mitochondrial dysfunction and cellular senescence. These findings establish aging in the
326 placenta as a feature of normal gestation; identify HIF-1 signaling as an upstream trigger
327 leading to mitochondrial dysfunction and senescence in the placenta; demonstrate that the
328 secretome of senescent trophoblasts is sufficient to potentiate uterine myocyte transformation
329 and contractility; and establish that HIF-1 induction *in vivo* can induce preterm labor. These
330 findings may have important implications for illuminating the factors that determine gestational
331 length both in health and disease.
332
333 **Data Availability:**
334 Statistics accompanying WGCNA (Figure 2) are accessible through Mendeley Data, doi:
335 10.17632/g6vrw9jjn4.1. (https://data.mendeley.com/datasets/g6vrw9jjn4/1)
336
337 The RNA Seq dataset has been deposited in NCBI's Gene Expression Omnibus[21] and is accessible
338 through GEO Series accession number GSE199278.
339 (https://www.ncbi.nlm.nih.gov/geo/query/acc.cgi?acc=GSE199278)
340
341 **Methods:**

342 *Mouse placenta collection:* C57BL/6 mice were fed a chow diet and housed at 20°C in a 12-hour
343 light/12-hour dark cycle. Nulliparous females (< 6 months of age) were housed for a single dark
344 cycle (midnight = gestational day 0) with a stud male. On gestational day e13.5-17.5, placentas
345 were isolated via laparotomy from pregnant females anesthetized via surgical-plane isoflurane.
346 Placentas were quartered, immersion-rinsed in dH_2O and blotted dry, then snap frozen in liquid
347 nitrogen and stored at -80°C prior to use.
348
349 *Mouse trophoblast isolation:* Protocol described in full in Pennington *et al*[69]. On gestational day
350 e15.5, placentas were collected via laparotomy from pregnant females anesthetized with
351 surgical-plane isoflurane. After dissection, placentas were quartered, immersion-rinsed in
352 dH2O, then placed in ice-cold digestion buffer: DMEM plus HEPES 20 mM, collagenase 1mg/mL,
353 and DNase I 4000U/mL. Placentas were digested for 20-40 minutes at 37°C with trituration and
354 examined under a microscope until optimal digestion achieved. Digested cells were passed
355 through a 70 micron strainer, washed in DMEM, then separated using a Percoll gradient.
356 Trophoblast fraction was washed once more then plated in complete medium: DMEM with
357 HEPES 20 mM, FBS 10%, and supplemented with sodium pyruvate, pen-strep-glutamine, non-
358 essential amino acids, and gentamicin.
359
360 *Mouse DMOG injection and measurement of gestational length*: On gestational day e16.5, dams
361 received an intraperitoneal injection of DMOG (Selleck Chemicals) 7.5 mg in 0.3 mL sterile
362 saline (approximately 250 mg/kg) versus vehicle alone. Video recordings were used to measure

363 gestational length, defined as interval from midnight of timed mating period until birth of the
364 first pup.
365
366 *Human placental specimens.* Placenta samples were collected at the time of cesarean delivery,
367 within 20 minutes of delivery of the placenta. Placental tissue was sampled from approximately
368 1cm deep to the maternal surface after dissecting away membranes. Cotyledons from all 4
369 quadrants were collected and minced together prior to immersion rinse in dH_2O and storage of
370 separate aliquots by snap freezing versus immersion in RNA Later. All samples were stored at -
371 80°C prior to use.
372
373 *Cell culture.*
374 JAR choriocarcinoma cells (ATCC) were grown in RPMI1640 media (4.5 g/L glucose) with 10%
375 FBS. Adherent JAR cells were treated with HIF1-stabilizing agents dissolved in 1X PBS (pH 7.4):
376 cobalt chloride hexahydrate (100 µM $CoCl_2$, Millipore Sigma) and dimethyloxalylglycine, N-
377 (methoxyoxoacetyl)-glycine methyl ester (1 mM DMOG, Millipore Sigma). JAR cells were
378 treated with 100 µM $CoCl_2$ or 1 mM DMOG in culture media as indicated prior to endpoint
379 assays.
380
381 Preparation of conditioned media: On day 5 of JAR cell treatment with $CoCl_2$ (versus control
382 condition), media exchange was performed to apply serum-free media for both conditions. 24
383 hours later, conditioned media samples were collected and applied to 10 kDa molecular weight
384 cutoff filters (Amicon Ultra), with centrifugation for 20 minutes at 4000 x *g*, 4°C. Filters were

385 washed with one volume of hTERT-HM base medium (see below), with repeat centrifugation.
386 Concentrated proteins retained in suspension above the filter were collected and stored at -
387 80°C.
388
389 hTERT-HM cells (generously supplied by Dr. Jennifer Condon, Wayne State) were grown in
390 DMEM/F12 medium (Gibco) with 10% FBS and Antibiotic-Antimycotic (1X, Gibco). Cells were
391 stimulated by addition of recombinant human IL-1 (R&D Systems) and/or filter-concentrated
392 JAR cell conditioned media as indicated, 6 hours prior to collection of cellular RNA.
393
394 *RT – qPCR*. Total RNA was reverse transcribed to cDNA with the Superscript III reverse
395 transcriptase (Invitrogen) system with random hexamer primers (Invitrogen) according to
396 manufacturer's instructions. cDNA was amplified via real-time quantitative PCR with TaqMan
397 Fast Advanced Master Mix (Applied Biosystems) or SYBR Green PCR Master mix (Qiagen) in a
398 QuantStudio 6 Flex Real-Time PCR System (Applied Biosystems). In mouse samples, target gene
399 expression was normalized to endogenous levels of housekeeping gene, β-actin. In human
400 samples, target gene expression was normalized to endogenous levels of housekeeping gene,
401 YWHAZ (TaqMan) or β-actin (SYBR). Mouse and human primers are listed in Table 2.
402
403 *Collagen lattice contraction assay*: As previously described[41,44], hTERT-HM cells were suspended
404 in a collagen gel matrix (Cellmatrix collagen type I-A, Fisher Scientific, prepared with MEM,
405 NaOH and HEPES) then plated in 12-well dishes and grown in hTERT-HM medium. When cells
406 reached approximately 60% confluence, gel matrix was detached from plate and experimental

407 treatments were applied in fresh cell culture medium. After 1 hour incubation, a photograph
408 was taken of each well for measurement of percent well area occupied by collagen disc,
409 reflecting cellular contraction.
410
411 *mtDNA damage assay.* Mitochondrial DNA damage was assayed from total DNA via a semi-long
412 run real-time PCR approach, as described elsewhere[32]. Briefly, separate qPCR reactions were
413 assayed to compare a long versus short amplicon representing each genomic region. A lesion
414 rate per 10 kb of mtDNA was calculated as:
415 lesion rate $= \frac{10000\ (bp)}{size\ of\ long\ fragment\ (bp)} * (1 - FC_{long-short})$,
416 with $FC_{long-short} = 2^{-\Delta\Delta Ct}$ calculated in the usual method.
417
418 *Relative mtDNA copy number.* qPCR assays for nuclear and mitochondrial genes were
419 performed using total DNA as a template. Relative mitochondrial DNA was calculated as:
420 follows:
421 mt:nuc DNA copy number $= 2 * 2^{\Delta Ct}$, where $\Delta Ct = Ct_{nuclear\ gene} - Ct_{mitochondrial\ gene}$.
422
423 *Immunoblots.* Antibodies are listed in Table 3.
424
425 *SA-β-Galactosidase Assay.* Adherent cells were fixed and stained for SA-βGal via a Senescence
426 Detection kit (Abcam, ab65351) per manufacturer's instructions. Representative images were
427 used to calculate the fraction of SA-β-Gal-positive cells, scored by an observer blinded to
428 treatment condition.

Table 2. Primers

Mouse

Target	Sequence	Platform
GLB1	Mm00515342_m1	TaqMan
HK-2	Mm00443385_m1	TaqMan
GLUT1	Mm00441473_m1	TaqMan
D loop (long, 801 bp amplicon)	F: CGTACATTAAACTATTTTCCCCAAG R: GAGTTTTGGTTCACGGAACAT	SYBR
COII/ATPase 6 (long, 855 bp amplicon)	F: TTGGTCTACAAGACGCCACA R: ATTTTGGTGAAGGTGCCAGT	SYBR
ND5 (long, 930 bp amplicon)	F: CGCCTACTCCTCAGTTAGCC R: ATGGTGACTCAGTGCCAGGT	SYBR
ND2/ND1 (long, 832 bp amplicon)	F: GGATGAGCCTCAAACTCCAA R: ATGATGGCAAGGGTGATAGG	SYBR
D loop (short)	F: TGACTATCCCCTTCCCCATT R: TTGTTGGTTTCACGGAGGAT	SYBR
COII/ATPase 6 (short)	F: TCTCCCCTCTCTACGCATTC R: CGGTTAATACGGGGTTGTTG	SYBR
ND5 (short)	F: GGCCTCACATCATCACTCCT R: GCTGTGGATCCGTTCGTAGT	SYBR
ND2/ND1 (short)	F: GGATGAGCCTCAAACTCCAA R: GGCTCGTAAAGCTCCGAATA	SYBR
ACTINB	Mm00607939_s1	TaqMan

Human

Target	Sequence	Platform
HK-2	Hs00606086_m1	TaqMan
GLUT1	Hs00892681_m1	TaqMan
IL-1α	Hs00174092_m1	TaqMan
IL-1β	Hs01555410_m1	TaqMan
TNFα	Hs00174128_m1	TaqMan
IL-6	Hs00174131_m1	TaqMan
IL-10	Hs00961622_m1	TaqMan
MT-ATP-6	Hs02596862_g1	TaqMan
MT-CO2	Hs02596865_g1	TaqMan
ND1	F: CCATAAAACCCGCCACACT R: GAGCGATGGTGAGAGCTAAGGT	SYBR
18S	F: CGCAGCTAGGAATAATGGAATAGG R: CATGGCCTCAGTTCCGAAA	SYBR
CNX43	Hs.PT.58.38338544	SYBR
COX2	Hs.PT.58.77266	SYBR
ACTB	Hs.PT.39a.22214847	SYBR
YWHAZ	Hs01122445_g1	TaqMan

Table 3. Antibodies

Target	Species	Working Concentration	Source
Cox IV	Mouse IgG mAb	1:1,000	Cell Signaling Technology, #11967S
β-Actin-HRP	Rabbit IgG mAb	1:2,000	Cell Signaling Technology, #5125S
HIF1	Rabbit	1:1000	Cell Signaling Technology, #14179S

429

430 *Live cell staining.* Adherent cells were stained using the TMRE-Mitochondrial Membrane
431 Potential Assay Kit (Abcam, ab113852) per manufacturer's instructions. Select wells were
432 pretreated with 20 µM FCCP, a decoupling agent, as a positive control for 20 minutes before
433 TMRE and Hoechst counterstain was applied. Live JAR cells were analyzed by the Celigo Image
434 Cytometer (Nexcelom BioScience) for fluorescence quantification and gating. Adherent live JAR
435 cells were stained with MitoSOX™ Red Mitochondrial Superoxide Indicator kit (Invitrogen) and
436 analyzed using the cytometer in a similar manner.

437

438 *Cell counting.* JAR cells were cultured for 6 days ± cobalt chloride exposure prior to cell
439 counting. On day 6, cells from each condition were replated in a 96-well plate in $CoCl_2$-free
440 media at a density of 5 x 10^3 cells per well. Celigo Image Cytometer was used for automated cell
441 counting (total cells per well) at 24-hour intervals.

442

443 *RNA-Seq.* Following 6 days of treatment with CoCl2 100 µM versus control media, total RNA was
444 isolated from JAR cells as described above. Extracted RNA (300ng) was treated with NEBNext
445 rRNA Depletion Kit v2 (E7400X) and cDNA was generated using random hexamer priming and
446 Maxima H Minus Reverse Transcriptase. cDNA was converted into double stranded cDNA using
447 NEBNext mRNA Second Strand Synthesis Module (E6111L) and sequencing libraries were
448 generated by tagmentation using Nextera XT DNA Library Preparation Kit (Illumina FC-131) with
449 12 cycles of PCR amplification. Sequencing libraries were analyzed by Qubit and Agilent

450 Bioanalyzer, pooled at a final concentration of 1.2pM, and sequenced on an Illumina
451 Nextseq500 instrument 36x8x36 read structure.
452
453 *Transcriptomics Analysis*: Sequencing reads were demultiplexed and trimmed for adapters
454 using bcl2fastq (v2.20.0). Secondary adapter trimming, NextSeq/Poly(G) tail trimming, and read
455 filtering was performed using fastp (v0.20.0)[70]; low quality reads and reads shorter than 18nt
456 after trimming were removed from the read pool. Salmon (v1.1.0)[71] was used to simultaneously
457 map and quantify reads to transcripts in the GENCODE 33 genome annotation of the
458 GRCh38/hg38 human assembly. Salmon was run using full selective alignment, with sequence-
459 specific and fragment GC-bias correction turned on (--seqBias and --gcBias options,
460 respectively). Transcript abundances were collated and summarized to gene abundances using
461 the tximport package for R[72]. Normalization and differential expression analysis were
462 performed using edgeR[73,74]. For differential gene expression analysis, genes were considered
463 significant if they passed a fold change (FC) cutoff of log2FC > 1 and a false discovery rate (FDR)
464 cutoff of FDR < 0.05. Functional enrichment analyses were performed using g:Profiler[75].
465 WGCNA[76] was performed after removing genes with low expression as previously described[77].
466
467 *Statistics.* Student's two-tailed unpaired t-test, ordinary one-way, and two-way ANOVA
468 statistical tests were applied as indicated to compare biological replicates in each experiment.
469
470 *Study Approval.* All animal experiments were approved by the Beth Israel Deaconess Medical
471 Center Institutional Animal Care and Use Committee. Human placental specimens and data

472 were biobanked and accessed under protocols approved by the Beth Israel Deaconess Medical
473 Center Institutional Review Board, and written informed consent was obtained before subject
474 participation.
475
476 **Author Contributions:**
477 EJC, LT, SAK, and SMP designed the studies. HS, CJ, and LT performed WCGNA and JAR cell
478 transcriptomic assay and analyses. EJC and PF conducted *in vitro*, human placenta, and mouse
479 experiments and analyzed their results. EJC, SAK, and SMP wrote the manuscript with input
480 and approval from all authors.
481
482 **Acknowledgements:**
483 We thank Dr. Jennifer Condon of Wayne State University School of Medicine for generously
484 providing the hTERT-HM cell line.
485
486 We thank Saira Salahuddin for maintaining the placenta biorepository and helping access the
487 study samples and accompanying clinical data.
488
489 Figures were created using Biorender.com.
490
491 Research reported in this publication was supported by the Institute of General Medical
492 Sciences of the National Institutes of Health under award GM007592-41 and the Foundation for
493 Anesthesia Education and Research (FAER) (EJC).
494

The authors declare no competing interests.

499 **References:**

500 1. Liu, L., Oza, S., Hogan, D., Perin, J., Rudan, I., Lawn, J.E., Cousens, S., Mathers, C., and
501 Black, R.E. (2015). Global, regional, and national causes of child mortality in 2000-13,
502 with projections to inform post-2015 priorities: an updated systematic analysis. Lancet
503 *385*, 430-440. 10.1016/S0140-6736(14)61698-6.

504 2. Blencowe, H., Cousens, S., Chou, D., Oestergaard, M., Say, L., Moller, A.B., Kinney, M.,
505 Lawn, J., and Born Too Soon Preterm Birth Action, G. (2013). Born too soon: the global
506 epidemiology of 15 million preterm births. Reprod Health *10 Suppl 1*, S2. 10.1186/1742-
507 4755-10-S1-S2.

508 3. Goldenberg, R.L., Culhane, J.F., Iams, J.D., and Romero, R. (2008). Epidemiology and
509 causes of preterm birth. Lancet *371*, 75-84. 10.1016/S0140-6736(08)60074-4.

510 4. Smith, V., Devane, D., Begley, C.M., Clarke, M., and Higgins, S. (2009). A systematic
511 review and quality assessment of systematic reviews of randomised trials of
512 interventions for preventing and treating preterm birth. Eur J Obstet Gynecol Reprod
513 Biol *142*, 3-11. 10.1016/j.ejogrb.2008.09.008.

514 5. Romero, R., Dey, S.K., and Fisher, S.J. (2014). Preterm labor: one syndrome, many
515 causes. Science *345*, 760-765. 10.1126/science.1251816.

516 6. Kiserud, T., Ebbing, C., Kessler, J., and Rasmussen, S. (2006). Fetal cardiac output,
517 distribution to the placenta and impact of placental compromise. Ultrasound Obstet
518 Gynecol *28*, 126-136. 10.1002/uog.2832.

519 7. Shaut, C.A., Keene, D.R., Sorensen, L.K., Li, D.Y., and Stadler, H.S. (2008). HOXA13 Is
520 essential for placental vascular patterning and labyrinth endothelial specification. PLoS
521 Genet *4*, e1000073. 10.1371/journal.pgen.1000073.
522 8. Lykke, J.A., Langhoff-Roos, J., Sibai, B.M., Funai, E.F., Triche, E.W., and Paidas, M.J.
523 (2009). Hypertensive pregnancy disorders and subsequent cardiovascular morbidity and
524 type 2 diabetes mellitus in the mother. Hypertension *53*, 944-951.
525 10.1161/HYPERTENSIONAHA.109.130765.
526 9. Genbacev, O., Joslin, R., Damsky, C.H., Polliotti, B.M., and Fisher, S.J. (1996). Hypoxia
527 alters early gestation human cytotrophoblast differentiation/invasion in vitro and
528 models the placental defects that occur in preeclampsia. J Clin Invest *97*, 540-550.
529 10.1172/JCI118447.
530 10. Plaks, V., Rinkenberger, J., Dai, J., Flannery, M., Sund, M., Kanasaki, K., Ni, W., Kalluri, R.,
531 and Werb, Z. (2013). Matrix metalloproteinase-9 deficiency phenocopies features of
532 preeclampsia and intrauterine growth restriction. Proc Natl Acad Sci U S A *110*, 11109-
533 11114. 10.1073/pnas.1309561110.
534 11. Li, F., Fushima, T., Oyanagi, G., Townley-Tilson, H.W., Sato, E., Nakada, H., Oe, Y.,
535 Hagaman, J.R., Wilder, J., Li, M., et al. (2016). Nicotinamide benefits both mothers and
536 pups in two contrasting mouse models of preeclampsia. Proc Natl Acad Sci U S A *113*,
537 13450-13455. 10.1073/pnas.1614947113.
538 12. Romero, R., and Chaiworapongsa, T. (2013). Preeclampsia: a link between trophoblast
539 dysregulation and an antiangiogenic state. J Clin Invest *123*, 2775-2777.
540 10.1172/JCI70431.

541 13. McIntyre, K.R., Vincent, K.M.M., Hayward, C.E., Li, X., Sibley, C.P., Desforges, M.,
542 Greenwood, S.L., and Dilworth, M.R. (2020). Human placental uptake of glutamine and
543 glutamate is reduced in fetal growth restriction. Sci Rep *10*, 16197. 10.1038/s41598-
544 020-72930-7.
545 14. Xu, Y.Y., Liu, Y., Cui, L., Wu, W.B., Quinn, M.J., Menon, R., and Zhang, H.J. (2021).
546 Hypoxic effects on the mitochondrial content and functions of the placenta in fetal
547 growth restriction. Placenta *114*, 100-107. 10.1016/j.placenta.2021.09.003.
548 15. Koga, K., Cardenas, I., Aldo, P., Abrahams, V.M., Peng, B., Fill, S., Romero, R., and Mor, G.
549 (2009). Activation of TLR3 in the trophoblast is associated with preterm delivery. Am J
550 Reprod Immunol *61*, 196-212. 10.1111/j.1600-0897.2008.00682.x.
551 16. Pique-Regi, R., Romero, R., Tarca, A.L., Sendler, E.D., Xu, Y., Garcia-Flores, V., Leng, Y.,
552 Luca, F., Hassan, S.S., and Gomez-Lopez, N. (2019). Single cell transcriptional signatures
553 of the human placenta in term and preterm parturition. Elife *8*. 10.7554/eLife.52004.
554 17. Beharier, O., Tyurin, V.A., Goff, J.P., Guerrero-Santoro, J., Kajiwara, K., Chu, T., Tyurina,
555 Y.Y., St Croix, C.M., Wallace, C.T., Parry, S., et al. (2020). PLA2G6 guards placental
556 trophoblasts against ferroptotic injury. Proc Natl Acad Sci U S A *117*, 27319-27328.
557 10.1073/pnas.2009201117.
558 18. Elshenawy, S., Pinney, S.E., Stuart, T., Doulias, P.T., Zura, G., Parry, S., Elovitz, M.A.,
559 Bennett, M.J., Bansal, A., Strauss, J.F., 3rd, et al. (2020). The Metabolomic Signature of
560 the Placenta in Spontaneous Preterm Birth. Int J Mol Sci *21*. 10.3390/ijms21031043.
561 19. Lien, Y.C., Zhang, Z., Cheng, Y., Polyak, E., Sillers, L., Falk, M.J., Ischiropoulos, H., Parry, S.,
562 and Simmons, R.A. (2021). Human Placental Transcriptome Reveals Critical Alterations in

563 Inflammation and Energy Metabolism with Fetal Sex Differences in Spontaneous
564 Preterm Birth. Int J Mol Sci *22*. 10.3390/ijms22157899.
565 20. Paquette, A.G., Brockway, H.M., Price, N.D., and Muglia, L.J. (2018). Comparative
566 transcriptomic analysis of human placentae at term and preterm delivery. Biol Reprod
567 *98*, 89-101. 10.1093/biolre/iox163.
568 21. Edgar, R., Domrachev, M., and Lash, A.E. (2002). Gene Expression Omnibus: NCBI gene
569 expression and hybridization array data repository. Nucleic Acids Res *30*, 207-210.
570 10.1093/nar/30.1.207.
571 22. Knox, K., and Baker, J.C. (2008). Genomic evolution of the placenta using co-option and
572 duplication and divergence. Genome Res *18*, 695-705. 10.1101/gr.071407.107.
573 23. Zhou, Q.Y., Fang, M.D., Huang, T.H., Li, C.C., Yu, M., and Zhao, S.H. (2009). Detection of
574 differentially expressed genes between Erhualian and Large White placentas on day 75
575 and 90 of gestation. BMC Genomics *10*, 337. 10.1186/1471-2164-10-337.
576 24. Loux, S.C., Dini, P., El-Sheikh Ali, H., Kalbfleisch, T., and Ball, B.A. (2019). Characterization
577 of the placental transcriptome through mid to late gestation in the mare. PLoS One *14*,
578 e0224497. 10.1371/journal.pone.0224497.
579 25. Soncin, F., Khater, M., To, C., Pizzo, D., Farah, O., Wakeland, A., Arul Nambi Rajan, K.,
580 Nelson, K.K., Chang, C.W., Moretto-Zita, M., et al. (2018). Comparative analysis of
581 mouse and human placentae across gestation reveals species-specific regulators of
582 placental development. Development *145*. 10.1242/dev.156273.
583 26. Maeda, K.J., Showmaker, K.C., Johnson, A.C., Garrett, M.R., and Sasser, J.M. (2019).
584 Spontaneous superimposed preeclampsia: chronology and expression unveiled by

585 temporal transcriptomic analysis. Physiol Genomics *51*, 342-355.
586 10.1152/physiolgenomics.00020.2019.
587 27. Morey, R., Farah, O., Kallol, S., Requena, D.F., Meads, M., Moretto-Zita, M., Soncin, F.,
588 Laurent, L.C., and Parast, M.M. (2021). Transcriptomic Drivers of Differentiation,
589 Maturation, and Polyploidy in Human Extravillous Trophoblast. Front Cell Dev Biol *9*,
590 702046. 10.3389/fcell.2021.702046.
591 28. Steinhauser, C.B., Lambo, C.A., Askelson, K., Burns, G.W., Behura, S.K., Spencer, T.E.,
592 Bazer, F.W., and Satterfield, M.C. (2021). Placental Transcriptome Adaptations to
593 Maternal Nutrient Restriction in Sheep. Int J Mol Sci *22*. 10.3390/ijms22147654.
594 29. Lee, B.Y., Han, J.A., Im, J.S., Morrone, A., Johung, K., Goodwin, E.C., Kleijer, W.J., DiMaio,
595 D., and Hwang, E.S. (2006). Senescence-associated beta-galactosidase is lysosomal beta-
596 galactosidase. Aging Cell *5*, 187-195. 10.1111/j.1474-9726.2006.00199.x.
597 30. Jang, J.Y., Blum, A., Liu, J., and Finkel, T. (2018). The role of mitochondria in aging. J Clin
598 Invest *128*, 3662-3670. 10.1172/JCI120842.
599 31. Trifunovic, A., Wredenberg, A., Falkenberg, M., Spelbrink, J.N., Rovio, A.T., Bruder, C.E.,
600 Bohlooly, Y.M., Gidlof, S., Oldfors, A., Wibom, R., et al. (2004). Premature ageing in mice
601 expressing defective mitochondrial DNA polymerase. Nature *429*, 417-423.
602 10.1038/nature02517.
603 32. Rothfuss, O., Gasser, T., and Patenge, N. (2010). Analysis of differential DNA damage in
604 the mitochondrial genome employing a semi-long run real-time PCR approach. Nucleic
605 Acids Res *38*, e24. 10.1093/nar/gkp1082.

606 33. Bratic, A., and Larsson, N.G. (2013). The role of mitochondria in aging. J Clin Invest *123*,
607 951-957. 10.1172/JCI64125.
608 34. Wiley, C.D., and Campisi, J. (2016). From Ancient Pathways to Aging Cells-Connecting
609 Metabolism and Cellular Senescence. Cell Metab *23*, 1013-1021.
610 10.1016/j.cmet.2016.05.010.
611 35. Wiley, C.D., and Campisi, J. (2021). The metabolic roots of senescence: mechanisms and
612 opportunities for intervention. Nat Metab *3*, 1290-1301. 10.1038/s42255-021-00483-8.
613 36. Maxwell, P.H., Wiesener, M.S., Chang, G.W., Clifford, S.C., Vaux, E.C., Cockman, M.E.,
614 Wykoff, C.C., Pugh, C.W., Maher, E.R., and Ratcliffe, P.J. (1999). The tumour suppressor
615 protein VHL targets hypoxia-inducible factors for oxygen-dependent proteolysis. Nature
616 *399*, 271-275. 10.1038/20459.
617 37. Jaakkola, P., Mole, D.R., Tian, Y.M., Wilson, M.I., Gielbert, J., Gaskell, S.J., von
618 Kriegsheim, A., Hebestreit, H.F., Mukherji, M., Schofield, C.J., et al. (2001). Targeting of
619 HIF-alpha to the von Hippel-Lindau ubiquitylation complex by O2-regulated prolyl
620 hydroxylation. Science *292*, 468-472. 10.1126/science.1059796.
621 38. Nursalim, Y.N.S., Blenkiron, C., Groom, K.M., and Chamley, L.W. (2020). Growing human
622 trophoblasts in vitro: a review of the media commonly used in trophoblast cell culture.
623 Reproduction *160*, R119-R128. 10.1530/REP-19-0605.
624 39. Rothbauer, M., Patel, N., Gondola, H., Siwetz, M., Huppertz, B., and Ertl, P. (2017). A
625 comparative study of five physiological key parameters between four different human
626 trophoblast-derived cell lines. Sci Rep *7*, 5892. 10.1038/s41598-017-06364-z.

627 40. Epstein, A.C., Gleadle, J.M., McNeill, L.A., Hewitson, K.S., O'Rourke, J., Mole, D.R.,
628 Mukherji, M., Metzen, E., Wilson, M.I., Dhanda, A., et al. (2001). C. elegans EGL-9 and
629 mammalian homologs define a family of dioxygenases that regulate HIF by prolyl
630 hydroxylation. Cell *107*, 43-54. 10.1016/s0092-8674(01)00507-4.
631 41. Nishimura, F., Mogami, H., Moriuchi, K., Chigusa, Y., Mandai, M., and Kondoh, E. (2020).
632 Mechanisms of thrombin-Induced myometrial contractions: Potential targets of
633 progesterone. PLoS One *15*, e0231944. 10.1371/journal.pone.0231944.
634 42. Rauk, P.N., and Chiao, J.P. (2000). Interleukin-1 stimulates human uterine prostaglandin
635 production through induction of cyclooxygenase-2 expression. Am J Reprod Immunol
636 *43*, 152-159. 10.1111/j.8755-8920.2000.430304.x.
637 43. Leimert, K.B., Verstraeten, B.S.E., Messer, A., Nemati, R., Blackadar, K., Fang, X.,
638 Robertson, S.A., Chemtob, S., and Olson, D.M. (2019). Cooperative effects of sequential
639 PGF2alpha and IL-1beta on IL-6 and COX-2 expression in human myometrial cellsdagger.
640 Biol Reprod *100*, 1370-1385. 10.1093/biolre/ioz029.
641 44. Devost, D., and Zingg, H.H. (2007). Novel in vitro system for functional assessment of
642 oxytocin action. Am J Physiol Endocrinol Metab *292*, E1-6.
643 10.1152/ajpendo.00529.2005.
644 45. Campisi, J., Kapahi, P., Lithgow, G.J., Melov, S., Newman, J.C., and Verdin, E. (2019).
645 From discoveries in ageing research to therapeutics for healthy ageing. Nature *571*, 183-
646 192. 10.1038/s41586-019-1365-2.
647 46. Rosso, P. (1976). Placenta as an aging organ. Curr Concepts Nutr *4*, 23-41.

648 47. Martin, B.J., and Spicer, S.S. (1973). Ultrastructural features of cellular maturation and
649 aging in human trophoblast. J Ultrastruct Res *43*, 133-149. 10.1016/s0022-
650 5320(73)90074-9.
651 48. Fox, H. (1997). Aging of the placenta. Arch Dis Child Fetal Neonatal Ed *77*, F171-175.
652 10.1136/fn.77.3.f171.
653 49. Sultana, Z., Maiti, K., Aitken, J., Morris, J., Dedman, L., and Smith, R. (2017). Oxidative
654 stress, placental ageing-related pathologies and adverse pregnancy outcomes. Am J
655 Reprod Immunol *77*. 10.1111/aji.12653.
656 50. Cindrova-Davies, T., Fogarty, N.M.E., Jones, C.J.P., Kingdom, J., and Burton, G.J. (2018).
657 Evidence of oxidative stress-induced senescence in mature, post-mature and
658 pathological human placentas. Placenta *68*, 15-22. 10.1016/j.placenta.2018.06.307.
659 51. Biron-Shental, T., Sukenik-Halevy, R., Sharon, Y., Goldberg-Bittman, L., Kidron, D., Fejgin,
660 M.D., and Amiel, A. (2010). Short telomeres may play a role in placental dysfunction in
661 preeclampsia and intrauterine growth restriction. Am J Obstet Gynecol *202*, 381 e381-
662 387. 10.1016/j.ajog.2010.01.036.
663 52. Chen, K.H., Chen, L.R., and Lee, Y.H. (2011). Exploring the relationship between preterm
664 placental calcification and adverse maternal and fetal outcome. Ultrasound Obstet
665 Gynecol *37*, 328-334. 10.1002/uog.7733.
666 53. Maiti, K., Sultana, Z., Aitken, R.J., Morris, J., Park, F., Andrew, B., Riley, S.C., and Smith, R.
667 (2017). Evidence that fetal death is associated with placental aging. Am J Obstet Gynecol
668 *217*, 441 e441-441 e414. 10.1016/j.ajog.2017.06.015.

669 54. Bonney, E.A., Krebs, K., Saade, G., Kechichian, T., Trivedi, J., Huaizhi, Y., and Menon, R.
670 (2016). Differential senescence in feto-maternal tissues during mouse pregnancy.
671 Placenta *43*, 26-34. 10.1016/j.placenta.2016.04.018.
672 55. Menon, R., Behnia, F., Polettini, J., Saade, G.R., Campisi, J., and Velarde, M. (2016).
673 Placental membrane aging and HMGB1 signaling associated with human parturition.
674 Aging (Albany NY) *8*, 216-230. 10.18632/aging.100891.
675 56. Menon, R., Richardson, L.S., and Lappas, M. (2019). Fetal membrane architecture, aging
676 and inflammation in pregnancy and parturition. Placenta *79*, 40-45.
677 10.1016/j.placenta.2018.11.003.
678 57. Hirota, Y., Daikoku, T., Tranguch, S., Xie, H., Bradshaw, H.B., and Dey, S.K. (2010).
679 Uterine-specific p53 deficiency confers premature uterine senescence and promotes
680 preterm birth in mice. J Clin Invest *120*, 803-815. 10.1172/JCI40051.
681 58. Hirota, Y., Cha, J., Yoshie, M., Daikoku, T., and Dey, S.K. (2011). Heightened uterine
682 mammalian target of rapamycin complex 1 (mTORC1) signaling provokes preterm birth
683 in mice. Proc Natl Acad Sci U S A *108*, 18073-18078. 10.1073/pnas.1108180108.
684 59. Nye, G.A., Ingram, E., Johnstone, E.D., Jensen, O.E., Schneider, H., Lewis, R.M.,
685 Chernyavsky, I.L., and Brownbill, P. (2018). Human placental oxygenation in late
686 gestation: experimental and theoretical approaches. J Physiol *596*, 5523-5534.
687 10.1113/JP275633.
688 60. Gomes, A.P., Price, N.L., Ling, A.J., Moslehi, J.J., Montgomery, M.K., Rajman, L., White,
689 J.P., Teodoro, J.S., Wrann, C.D., Hubbard, B.P., et al. (2013). Declining NAD(+) induces a

690 pseudohypoxic state disrupting nuclear-mitochondrial communication during aging. Cell
691 *155*, 1624-1638. 10.1016/j.cell.2013.11.037.
692 61. Gonzalez, T.L., Eisman, L.E., Joshi, N.V., Flowers, A.E., Wu, D., Wang, Y., Santiskulvong,
693 C., Tang, J., Buttle, R.A., Sauro, E., et al. (2021). High-throughput miRNA sequencing of
694 the human placenta: expression throughout gestation. Epigenomics *13*, 995-1012.
695 10.2217/epi-2021-0055.
696 62. Sferruzzi-Perri, A.N., Higgins, J.S., Vaughan, O.R., Murray, A.J., and Fowden, A.L. (2019).
697 Placental mitochondria adapt developmentally and in response to hypoxia to support
698 fetal growth. Proc Natl Acad Sci U S A *116*, 1621-1626. 10.1073/pnas.1816056116.
699 63. Albers, R.E., Kaufman, M.R., Natale, B.V., Keoni, C., Kulkarni-Datar, K., Min, S., Williams,
700 C.R., Natale, D.R.C., and Brown, T.L. (2019). Trophoblast-Specific Expression of Hif-
701 1alpha Results in Preeclampsia-Like Symptoms and Fetal Growth Restriction. Sci Rep *9*,
702 2742. 10.1038/s41598-019-39426-5.
703 64. Rasmussen, S., Ebbing, C., and Irgens, L.M. (2017). Predicting preeclampsia from a
704 history of preterm birth. PLoS One *12*, e0181016. 10.1371/journal.pone.0181016.
705 65. Mando, C., De Palma, C., Stampalija, T., Anelli, G.M., Figus, M., Novielli, C., Parisi, F.,
706 Clementi, E., Ferrazzi, E., and Cetin, I. (2014). Placental mitochondrial content and
707 function in intrauterine growth restriction and preeclampsia. Am J Physiol Endocrinol
708 Metab *306*, E404-413. 10.1152/ajpendo.00426.2013.
709 66. Fujimaki, A., Watanabe, K., Mori, T., Kimura, C., Shinohara, K., and Wakatsuki, A. (2011).
710 Placental oxidative DNA damage and its repair in preeclamptic women with fetal growth
711 restriction. Placenta *32*, 367-372. 10.1016/j.placenta.2011.02.004.

712 67. Davy, P., Nagata, M., Bullard, P., Fogelson, N.S., and Allsopp, R. (2009). Fetal growth
713 restriction is associated with accelerated telomere shortening and increased expression
714 of cell senescence markers in the placenta. Placenta *30*, 539-542.
715 10.1016/j.placenta.2009.03.005.
716 68. Burton, G.J., Yung, H.W., Cindrova-Davies, T., and Charnock-Jones, D.S. (2009). Placental
717 endoplasmic reticulum stress and oxidative stress in the pathophysiology of unexplained
718 intrauterine growth restriction and early onset preeclampsia. Placenta *30 Suppl A*, S43-
719 48. 10.1016/j.placenta.2008.11.003.
720 69. Pennington, K.A., Schlitt, J.M., and Schulz, L.C. (2012). Isolation of primary mouse
721 trophoblast cells and trophoblast invasion assay. J Vis Exp, e3202. 10.3791/3202.
722 70. Chen, S., Zhou, Y., Chen, Y., and Gu, J. (2018). fastp: an ultra-fast all-in-one FASTQ
723 preprocessor. Bioinformatics *34*, i884-i890. 10.1093/bioinformatics/bty560.
724 71. Patro, R., Duggal, G., Love, M.I., Irizarry, R.A., and Kingsford, C. (2017). Salmon provides
725 fast and bias-aware quantification of transcript expression. Nat Methods *14*, 417-419.
726 10.1038/nmeth.4197.
727 72. Soneson, C., Love, M.I., and Robinson, M.D. (2015). Differential analyses for RNA-seq:
728 transcript-level estimates improve gene-level inferences. F1000Res *4*, 1521.
729 10.12688/f1000research.7563.2.
730 73. Robinson, M.D., McCarthy, D.J., and Smyth, G.K. (2010). edgeR: a Bioconductor package
731 for differential expression analysis of digital gene expression data. Bioinformatics *26*,
732 139-140. 10.1093/bioinformatics/btp616.

733 74. Chen, Y., Lun, A.T., and Smyth, G.K. (2016). From reads to genes to pathways:
734 differential expression analysis of RNA-Seq experiments using Rsubread and the edgeR
735 quasi-likelihood pipeline. F1000Res *5*, 1438. 10.12688/f1000research.8987.2.
736 75. Raudvere, U., Kolberg, L., Kuzmin, I., Arak, T., Adler, P., Peterson, H., and Vilo, J. (2019).
737 g:Profiler: a web server for functional enrichment analysis and conversions of gene lists
738 (2019 update). Nucleic Acids Res *47*, W191-W198. 10.1093/nar/gkz369.
739 76. Langfelder, P., and Horvath, S. (2008). WGCNA: an R package for weighted correlation
740 network analysis. BMC Bioinformatics *9*, 559. 10.1186/1471-2105-9-559.
741 77. Bentsen, M.A., Rausch, D.M., Mirzadeh, Z., Muta, K., Scarlett, J.M., Brown, J.M.,
742 Herranz-Perez, V., Baquero, A.F., Thompson, J., Alonge, K.M., et al. (2020).
743 Transcriptomic analysis links diverse hypothalamic cell types to fibroblast growth factor
744 1-induced sustained diabetes remission. Nat Commun *11*, 4458. 10.1038/s41467-020-
745 17720-5.
746